Network-Based Epidemic Control Through Optimal Travel and Quarantine Management

Mahtab Talaei, Apostolos I. Rikos, Alex Olshevsky, Laura F. White, and Ioannis Ch. Paschalidis

***Abstract*—Motivated by the swift global transmission of infectious diseases, we present a comprehensive framework for network-based epidemic control. Our aim is to curb epidemics using two different approaches. In the first approach, we introduce an optimization strategy that optimally reduces travel rates. We analyze the convergence of this strategy and show that it hinges on the network structure to minimize infection spread. In the second approach, we expand the classic SIR model by incorporating and optimizing quarantined states to strategically contain the epidemic. We show that this problem reduces to the problem of matrix balancing. We establish a link between optimization constraints and the epidemic's reproduction number, highlighting the relationship between network structure and disease dynamics. We demonstrate that applying augmented primal-dual gradient dynamics to the optimal quarantine problem ensures exponential convergence to a stationary point. We conclude by validating our approaches using simulation studies that leverage public data from counties in the state of Massachusetts.**

***Index Terms*—Epidemics, networked control systems, stability of nonlinear systems, compartmental models, optimization.**

I. Introduction

THE recent COVID-19 pandemic underscored the critical importance of controlling infectious disease spread [1], [2]. Epidemics, when analyzed as interconnected networks (e.g., cities, counties, or other societal structures), pose significant challenges in preserving societal continuity and minimizing socio-economic disruptions. Control systems methods provide valuable tools for designing effective policies to mitigate the impact of epidemics on public health, economies, and society [3], [4].

Network-based epidemic models often adopt a compartmental approach, categorizing individuals into groups such as susceptible, infected, and recovered [3], [4]. Control methods in the literature primarily focus on *optimal control* and *spectral optimization*. Optimal control optimizes model parameters to minimize costs like the number of infections [5]–[9]. Spectral optimization addresses resource allocation by minimizing the maximum eigenvalue of the system matrix to limit spread [10]–[13]. However, given the complexity of epidemic models, designing and implementing policies to help mitigate the effects of an epidemic is computationally expensive and/or NP-hard (e.g., from the perspective of spectral optimization, the optimal node and link removal problems are NP-complete and NP-hard, respectively [14]). Recent work sought computationally efficient control strategies [15], [16]. Building on these efforts, our goal is to develop efficient frameworks for epidemic control that optimize resource allocation and minimize societal impact.

Main Contributions. We propose two novel strategies for network-based epidemic control. The first leverages optimal control principles by optimizing model input parameters to minimize an integrated cost function along the model trajectory. The second draws on spectral optimization to allocate resources efficiently, minimizing the spectral abscissa of the model's matrix for performance guarantees. Both strategies rely on controlling the dominant eigenvalue of the system matrix—one via travel restrictions and the other through quarantine measures—to establish effective outbreak control mechanisms. Our contributions are as follows:

- *Optimizing Travel Rates:* We introduce a novel approach to suppress epidemic spread by optimizing travel rates between network nodes (see Sec. IV). We analyze convergence and show that this method curbs disease transmission while preserving socio-economic activities by minimizing the dominant eigenvalue of the infection spread matrix. This underscores the centrality of the network analysis in epidemic control.
- *Optimizing Quarantine Rates:* We extend the SIR model to the SIQR model by incorporating a quarantine strategy for both asymptomatic and symptomatic individuals (see Sec. V). For the SIQR model, we demonstrate that optimizing quarantine costs becomes a matrix balancing problem solvable in polynomial time. Furthermore, We clarify how problem constraints relate to the basic reproduction number. As an extension, we show that augmented primal-dual dynamics yield semi-global exponential convergence to a stationary (KKT) point of the quarantine optimization problem.
- *Model Validation:* We validate the effectiveness of our approaches using real-world network data (cf. Sec. VI), computing optimal travel and quarantine rates for Massachusetts counties to illustrate the practical utility of our strategies.

Paper Organization. The rest of this article is organized as follows. In Sec. II we review necessary notation and background, and in Sec. III we outline our problem formulation. Sec. IV details our approach for epidemic control by optimizing travel rates. In Sec. V we introduce our extension of the SIR model to consider quarantined individuals, and we

Research partially supported by the NSF under grants DEB-2433726, ECCS-2317079, CCF-2200052, and IIS-1914792, by the ONR under grant N00014-19-1-2571, by the DOE under grant DE-AC02-05CH11231, by the NIH under grant UL54 TR004130, and by Boston University.

M. Talaei, A.I. Rikos, A. Olshevsky, and I.Ch. Paschalidis are with the Department of Electrical and Computer Engineering, and the Division of Systems Engineering, Boston University, Boston, MA, USA. E-mails: {mtalaei, arikos, alexols, yannisp}@bu.edu. I.Ch. Paschalidis is also affiliated with the Department of Biomedical Engineering and the Faculty for Computing & Data Sciences, Boston University, Boston, MA, USA.

L.F. White is with the School of Public Health, Boston University, Boston, MA, USA, e-mail: lfwhite@bu.edu.

The results in this paper were not presented at any conference.

demonstrate how epidemic control is achievable by optimizing quarantine rates. Finally, in Sec. VI we present numerical results obtained from simulations on networks using publicly available data from Massachusetts counties.

II. Notation and Preliminaries

The sets of real, integer, complex, and natural numbers are denoted by $\mathbb{R}$, $\mathbb{Z}$, $\mathbb{C}$, and $\mathbb{N}$, respectively. $\mathbb{R}_{\geq 0}$ ($\mathbb{R}_{>0}$) refers to nonnegative (positive) real numbers, and $\mathbb{R}_{\leq 0}$ ($\mathbb{R}_{<0}$) refers to nonpositive (negative) real numbers. Vectors and matrices are denoted by lowercase and capital letters, respectively. For a matrix $A \in \mathbb{R}^{n\times n}$, the entry at row i and column j is denoted by a_{ij}. The column vector concatenating all columns of A into a single column is $a = \text{vec}(A)$. Vectors are assumed to be column vectors unless stated otherwise. The standard basis of $\mathbb{R}^n$ is denoted by $\{e_i\}_{i=1}^n$. $\mathbf{1}$ denotes the all-ones column vector, I the identity matrix, and $\mathbf{0}$ the all-zero vector or matrix. Inequalities between vectors are elementwise. A matrix is nonnegative (nonpositive, negative, positive) if all its elements are nonnegative (nonpositive, negative, positive). A matrix is essentially nonnegative if all off-diagonal elements are nonnegative. The dominant eigenvalue and eigenvector of a matrix A are $\lambda_{\max}(A)$ and $u_{\max}(A)$. For a vector a, $\|a\|$ is its Euclidean norm, and $\text{diag}(a)$ is a diagonal matrix with a as the diagonal elements. The element-wise multiplication of two vectors a and b is $a \circ b$. The transpose, spectral radius, inverse, and Moore-Penrose inverse of a matrix A are denoted by A^T, $\rho(A)$, A^{-1}, and A^+. The complex conjugate of A is $\bar{A}$, and its conjugate transpose is A^*. The spectral norm of a square matrix A is $\|A\|_2 = \lambda_{\max}(A^*A)^{\frac{1}{2}}$. The derivative of a variable s with respect to time t is denoted by $\dot{s}$. The gradient of a function f is written as ∇f. A function is L-smooth if it is continuously differentiable with a Lipschitz continuous gradient having Lipschitz constant L. A neighborhood $\mathcal{N}(Z_0)$ of a matrix $Z_0 \in \mathbb{C}^{n\times n}$ is a set of matrices close to Z_0 in some metric. For $x \in \mathbb{R}$, $[x]_+ := \max\{x, 0\}$.

The network is represented by a *directed graph (digraph)*, denoted as $\mathcal{G} = (\mathcal{V}, \mathcal{E})$. In $\mathcal{G}$, the set of nodes is expressed as $\mathcal{V} = \{v_1, \ldots, v_n\}$, and the set of edges is defined as $\mathcal{E} \subseteq \{\mathcal{V} \times \mathcal{V} \cup (v_i, v_i) \mid v_i \in \mathcal{V}\}$, where each node has a virtual self-edge. The number of nodes and edges are denoted as $|\mathcal{V}| = n$ and $|\mathcal{E}| = m$, respectively. A *directed path* of length t exists from node v_i to node v_l if there is a sequence of nodes $v_i \equiv l_0, l_1, \ldots, l_t \equiv v_l$ such that $(l_\tau, l_{\tau+1}) \in \mathcal{E}$ for $\tau = 0, 1, \ldots, t-1$. A digraph is called "strongly connected" if there is a directed path from every node v_i to every other node v_l for all pairs of nodes $v_i, v_l \in \mathcal{V}$. A square nonnegative matrix $A \in \mathbb{R}_{\geq 0}^{n\times n}$ corresponds to a digraph $G(A)$ with n nodes $\{v_1, \ldots, v_n\}$ and a set edges $\mathcal{E} = \{(v_i, v_j) \mid a_{ij} > 0\}$.

Definition 1 (Strongly Connected Matrix)**.** *A square nonnegative matrix A is said to be strongly connected if its corresponding digraph $G(A)$ is strongly connected.*

Definition 2 (Primitive Matrix)**.** *A primitive matrix is a square nonnegative matrix some power of which is positive.*

Definition 3 (Matrix Stability and Function Convergence)**.** *A matrix A is called* continuous-time stable *if all its eigenvalues have real parts less than or equal to zero. A matrix A is called* discrete-time stable *if all its eigenvalues have magnitudes less than or equal to one. A function $y(t)$ is said to* decay at rate $\alpha \geq 0$ *starting at t_0 if $y(t) \leq y(t_0)\, e^{-\alpha\,(t-t_0)}$, for all $t \geq t_0$. Here, α is a constant that quantifies the exponential rate of decay.*

A. Network spread model of COVID-19

To model COVID-19 spread, we use a nuanced extension of the basic Susceptible-Infected-Recovered (SIR) model by separating the infected individuals into symptomatic and asymptomatic compartments (see [15], [17], [18] and references therein). This division captures differing epidemiological dynamics, such as infectiousness and detection rates between these subgroups. The proposed model is:

$$\dot{s}_i = -s_i \sum_{j=1}^{n} a_{ij}(\beta^{\text{a}} x_j^{\text{a}} + \beta^{\text{s}} x_j^{\text{s}}), \tag{1a}$$

$$\dot{x}_i^{\text{a}} = s_i \sum_{j=1}^{n} a_{ij}(\beta^{\text{a}} x_j^{\text{a}} + \beta^{\text{s}} x_j^{\text{s}}) - (\epsilon + r^{\text{a}}) x_i^{\text{a}}, \tag{1b}$$

$$\dot{x}_i^{\text{s}} = \epsilon x_i^{\text{a}} - r^{\text{s}} x_i^{\text{s}}, \tag{1c}$$

$$\dot{h}_i = r^{\text{a}} x_i^{\text{a}} + r^{\text{s}} x_i^{\text{s}}, \tag{1d}$$

where n is the number of locations in our network, $s = (s_1, \ldots, s_n) \in \mathbb{R}^n$ is a vector with elements s_i equal to the proportion of the population at location i being susceptible, x^{a} and x^{s} are vectors with elements equal to the proportion of the population at each location being asymptomatic and symptomatic, respectively, and h is the vector with elements h_i denoting the portion of recovered population at node i. a_{ij} is the rate at which infections at location j affect those at location i (to be computed later), β^{a} and β^{s} are the disease transmission rates of asymptomatic and symptomatic individuals, respectively, r^{a} and r^{s} are the recovery rates of asymptomatic and symptomatic, respectively, and ϵ is the rate at which asymptomatic individuals develop symptoms.

Following [15], different parameters are utilized for symptomatic and asymptomatic individuals due to the findings of [19]. Specifically, in [19] it is shown that asymptomatic individuals exhibit a more rapid decline in viral load (compared to symptomatic). Consequently, not only do they experience quicker recovery, but they are also likely to be less contagious.

Remark 1. *Model (1) offers a versatile framework. It can be reduced to SIR or SEIR models (by setting $\beta^{\text{s}} = r^{\text{s}} = \epsilon = 0$, or $\beta^{\text{a}} = r^{\text{a}} = 0$, respectively), but its main advantage lies in its extensibility, which is a key focus of this paper.*

B. Construction of Infection Flow and Travel Rates Matrices

Infection Flow Matrix. To construct the infection flow matrix A, we adopt the approach from [15], [18], which is particularly suited for modeling the impact of mobility restrictions during COVID-19. At each location i, the fixed population size is denoted by N_i, and people travel from location i to location j at a rate τ_{ij}. The travel rate matrix $T = [\tau_{ij}]_{i,j=1}^n$ is thus an $n \times n$ matrix. Travel rates play a pivotal role in determining the

evolution of an epidemic, as evidenced by [20], which highlighted the strong correlation between regional disease spread and human mobility. For instance, [21], [22] demonstrated how spatial movements between network subpopulations critically influence disease propagation, leveraging these concepts to analyze and predict epidemic dynamics.

The adjacency matrix A, however, does not depend solely on raw travel rates. Instead, it represents the *effective contact rate* between susceptible and infected individuals across locations. This follows principles established in metapopulation models of epidemic spread [23], [24] and reflects recent advances [18], [25]. Specifically, new infections arise due to interactions between susceptibles and infected individuals either within the same subpopulation or during visits to neighboring subpopulations. The effective contact rate is defined as the ratio of the time infected (asymptomatic and symptomatic) individuals (local and visiting) spend outside ($\sum_{j=1}^{n} N_j \tau_{jl} x_j^a$ and $\sum_{j=1}^{n} N_j \tau_{jl} x_j^s$, respectively) to the total time all individuals spend outside in a given location ($\sum_{k=1}^{n} N_k \tau_{kl}$). Formally, τ_{ij} combines with the effective contact rate at subpopulation j to build the rate of change for the susceptible individuals at location i:

$$\dot{s}_i = -\sum_{l=1}^{n} s_i \tau_{il} \left(\frac{\sum_{j=1}^{n} N_j \tau_{jl} x_j^a}{\sum_{k=1}^{n} N_k \tau_{kl}} \beta^a + \frac{\sum_{j=1}^{n} N_j \tau_{jl} x_j^s}{\sum_{k=1}^{n} N_k \tau_{kl}} \beta^s \right). \tag{2}$$

Thus, comparing (2) with (1a), we can define

$$a_{ij} = \sum_{l=1}^{n} \tau_{il} \tau_{jl} \frac{N_j}{\sum_{k=1}^{n} N_k \tau_{kl}}. \tag{3}$$

Travel Rates. To construct the travel rate matrix T, we utilize the Human Mobility Flow dataset [26], derived from SafeGraph data during the COVID-19 pandemic. This dataset captures daily visitor flows between *Census Block Groups (CBGs)* and provides population flow estimates reflecting general mobility patterns. It also generates the estimates for the whole population CBG-to-CBG flow. In our simulations, we focus on county-level trips within Massachusetts, aggregating flows within and between counties. The travel rate τ_{ij} is computed as:

$$\tau_{ij} = t_i \frac{P_f(i,j)}{\sum_k P_f(i,k)},$$

where P_f is the population flow matrix, and $P_f(i,j)$ represents the number of daily trips from location i to j. Here, t_i represents the fraction of time individuals from node i spend outside their residences. This formulation, rooted in real-time mobility data, is adaptable to various spatial scales (e.g., counties, census tracts) and allows for flexible modeling of heterogeneous disease spread dynamics.

By integrating origin-to-destination mobility patterns with effective contact rates, our framework provides a robust foundation for analyzing epidemic spread and control across interconnected networks.

C. Stability and Splitting of Matrices

We now provide the following lemmas about the stability of matrices that is important for our subsequent development.

Lemma 1 (A Perron–Frobenius version from [15])**.** *Suppose A is strongly connected with nonnegative off-diagonal entries. Then A has a unique (simple) real eigenvalue $\lambda_{\max}(A)$ that strictly dominates all other in real part. Moreover, its corresponding eigenvector $u_{\max}(A)$ is real and positive.*

Lemma 2 ([15])**.** *The following statements characterize continuous and discrete-time matrix stability.*

- *(Continuous-time stability). A strongly connected matrix P with nonnegative off-diagonal elements is continuous-time stable if and only if there exists a vector $d > \mathbf{0}$ such that $Pd \leq \mathbf{0}$.*
- *(Discrete-time stability). A nonnegative strongly connected matrix B is discrete-time stable if and only if there exists a vector $d > \mathbf{0}$ such that $Bd \leq d$.*
- *(Connection between Continuous-time and Discrete-time stability). Suppose $P = L - D$ where L is a nonnegative matrix while D is a matrix with nonpositive off-diagonal elements whose inverse is elementwise nonnegative. Suppose further that both P and $D^{-1}L$ are strongly connected. Then P is continuous-time stable if and only if $B = D^{-1}L$ is discrete-time stable.*

Lemma 1 restates Perron–Frobenius theorem for strongly connected, essentially nonnegative matrices. Lemma 2 characterizes matrix stability for both a continuous-time and a discrete-time setting, establishing relationships between matrix properties and stability conditions.

D. Balancing of Nonnegative Matrices

Matrix balancing adjusts elements of a given matrix to meet specific criteria. A square matrix $A \in \mathbb{R}_{\geq 0}^{n \times n}$ is balanced if $A\mathbf{1} = A^T\mathbf{1}$, meaning each row sum equals the corresponding column sum. A nonnegative matrix $A \in \mathbb{R}_{\geq 0}^{n \times n}$ can be balanced if and only if it is strongly connected [27]. Balancing A is equivalent to finding a nonnegative diagonal matrix D such that DAD^{-1} is balanced.

Early works [28] considered matrix balancing as a condition for a sequence of matrices to converge to a doubly stochastic limit. More recent studies [29] approached balancing a given matrix in a distributed manner, treating each row(/column) as the set of incoming(/outgoing) links of a network node (see [30] for a survey). We rely on the method from [31], which shows that matrix balancing can be achieved in linear time. Following this work, we state that the complexity is proportional to the number of nonzero matrix entries (as discussed in [15, Sec. 2.2]).

III. Problem Formulation

Our goal is to optimally modify the elements of the COVID-19 model (cf. Sec. 1) in a non-uniform way to mitigate disease spread while minimizing economic costs. We focus on two interrelated problems, denoted by **P1** and **P2**:

P1 In the first problem, we aim to optimally modify the travel rate matrix T (e.g., by implementing limited travel restrictions) to curb infection spread (see Section IV).

P2 In the second problem, we extend the COVID-19 model (cf. (1)) to include quarantined individuals. We then

optimally select location-dependent quarantine rates to curb infections while minimizing associated economic costs (see Section V).

Although **P1** and **P2** employ different control measures—travel restrictions and quarantines—they share a common technical foundation. Both problems reduce epidemic control to established optimization frameworks by leveraging network properties and spectral characteristics. This unified approach ensures a coherent strategy for outbreak management, where insights and methods from one problem inform and strengthen the solution to the other.

IV. Optimal Travel Rates for Epidemic Control

A. Problem Structure

The network spread model of COVID-19 in (1) can be written in matrix form as

$$\begin{pmatrix} \dot{s} \\ \dot{x}^{\mathrm{a}} \\ \dot{x}^{\mathrm{s}} \\ \dot{h} \end{pmatrix} = \begin{pmatrix} \mathbf{0} & -\beta^{\mathrm{a}} \operatorname{diag}(s) A & -\beta^{\mathrm{s}} \operatorname{diag}(s) A & \mathbf{0} \\ \mathbf{0} & C & \beta^{\mathrm{s}} \operatorname{diag}(s) A & \mathbf{0} \\ \mathbf{0} & \epsilon I & -r^{\mathrm{s}} I & \mathbf{0} \\ \mathbf{0} & r^{\mathrm{a}} I & r^{\mathrm{s}} I & \mathbf{0} \end{pmatrix} \begin{pmatrix} s \\ x^{\mathrm{a}} \\ x^{\mathrm{s}} \\ h \end{pmatrix}, \tag{4}$$

where $C = \beta^{\mathrm{a}} \operatorname{diag}(s) A - (\epsilon + r^{\mathrm{a}}) I$. We consider matrix A as a function of $\tau = \operatorname{vec}(T)$, where T is the travel matrix (cf. Sec. II-B). Under Assumptions 1 and 2 in [12], we can decouple the dynamics of $\dot{x}$ from $\dot{s}$ and $\dot{h}$ in (4), isolating the infected compartments. This results in the infected system matrix $M(t, \tau)$, which depends on time and travel rates. By substituting the initial susceptible rate $s(t_0)$ into the system, we obtain

$$M(t_0, \tau) = \begin{pmatrix} C' & \beta^{\mathrm{s}} \operatorname{diag}(s(t_0)) A(\tau) \\ \epsilon I & -r^{\mathrm{s}} I \end{pmatrix}, \tag{5}$$

where C' depends on $A(\tau)$ and is defined as $\beta^{\mathrm{a}} \operatorname{diag}(s(t_0)) A(\tau) - (\epsilon + r^{\mathrm{a}}) I$. For a fixed t_0, we define $f(\tau) = \lambda_{\max}(M(t_0, \tau))$, and aim to solve the following minimization problem:

$$\begin{aligned} \min_{\tau} \quad & f(\tau) \\ \text{s.t.} \quad & \|\tau - \tau_0\|_1 \le b, \\ & \tau \ge \mathbf{0} \end{aligned} \tag{6}$$

where τ_0 is the vector of initial travel rates and b is a budget on the amount of travel rate change (measured using an ℓ_1 norm) from their initial values. The parameter b prevents drastic changes in travel rates, mitigating potential social disruption. This constraint ensures the practical feasibility of travel rate adjustments.

In (6), we focus on minimizing the dominant eigenvalue of the matrix $M(t_0, \tau)$ by optimizing travel rates. In particular, minimizing the dominant eigenvalue of the infected system matrix is a powerful strategy for curbing the spread of infection. The formal justification for this approach is provided in the following proposition.

Proposition 1. *Consider the infected system matrix $M(t_0)$ from (5). If the dominant eigenvalue of $M(t_0)$ is minimized such that $\lambda_{\max}(M(t_0)) < -\alpha$ for some $\alpha > 0$ at time t_0, then the number of infected cases decays to zero at rate α, that is, bounded asymptotically by a multiple of $e^{-\alpha t}$ for all $t \ge t_0$.*

Proof. The proof of Proposition 1 is established in [15]. □

B. Proposed Solution

We apply *Projected Gradient Descent (PGD)* by projecting onto the constraint set, specifically the nonnegative orthant of the ℓ_1 ball. To ensure convergence, we use a backtracking line search to adaptively adjust the stepsize based on sufficient decrease conditions, enhancing robustness and convergence (see [32]). The proposed algorithm is as follows:

$$\begin{aligned} &\textit{Initialization:} \\ &\text{set } \gamma = 1 \text{ and choose } \beta \in (0,1), \\ &\textit{Iteration:} \\ &\text{while } f(\tau_k - \gamma \nabla f(\tau_k)) > f(\tau_k) - \frac{\gamma}{2} \|\nabla f(\tau_k)\|^2, \\ &\quad \text{set } \gamma \leftarrow \beta\gamma, \\ &y_{k+1} = \tau_k - \gamma \nabla f(\tau_k), \\ &\tau_{k+1} = \arg\min_{\tau \in \Omega} \|\tau - y_{k+1}\|_2^2, \end{aligned} \tag{7}$$

where γ is the stepsize adjusted via backtracking with scaling factor $\beta \in (0,1)$, $\tau_k = \operatorname{vec}(T_k)$ represents the vectorized travel rates matrix at iteration k, Ω is the projection set, and y_{k+1} is the auxiliary variable before projection onto the ℓ_1 ball.

The update in (7) involves a gradient descent step followed by projection onto the feasible set Ω. Computing the gradient of the maximum eigenvalue requires specialized techniques, while the projection step ensures the travel rates remain practical and realistic under the imposed constraints.

Gradient Descent Step. Computing the gradient of a matrix maximum eigenvalue can be challenging [33]. To address this, we use [34, Thm. 2], which states:

Theorem 1 ([34])**.** *Let λ_0 be a simple eigenvalue of a matrix $Z_0 \in \mathbb{C}^{n \times n}$, with u_0 as an associated eigenvector, such that $Z_0 u_0 = \lambda_0 u_0$. Then a (complex) function λ and a (complex) vector function u are defined for all Z in some neighborhood $\mathcal{N}(Z_0) \in \mathbb{C}^{n \times n}$ of Z_0, such that $\lambda(Z_0) = \lambda_0$, $u(Z_0) = u_0$, and*

$$Zu = \lambda u, \ u_0^* u = 1, \text{ for } Z \in \mathcal{N}(Z_0).$$

Moreover, the functions λ and u are ∞ times differentiable on $\mathcal{N}(Z_0)$ and the differentials at Z_0 are

$$d\lambda = v_0^*(dZ)u_0 / v_0^* u_0 \ , \tag{8}$$

and

$$du = (\lambda_0 I - Z_0)^+ \left(I - \frac{u_0 v_0^*}{v_0^* u_0} \right) (dZ) u_0 \ , \tag{9}$$

where v_0 is the eigenvector associated with the eigenvalue $\bar{\lambda}_0$ of Z_0^*, satisfying $Z_0^* v_0 = \bar{\lambda}_0 v_0$, and dZ is the differential of Z.

Let $Z_0 = M(t_0, \tau_k)$ in Theorem 1, with $\lambda_{\max}$ and $u_{\max}$ denoting the maximum eigenvalue and its corresponding eigenvector, such that $M(t_0, \tau_k) u_{\max} = \lambda_{\max} u_{\max}$. In a

neighborhood $\mathcal{N}(M(t_0,\tau_k)) \in \mathbb{C}^{n\times n}$, there exists a function f satisfying $f(M(t_0,\tau_k)) = \lambda_{\max}$, and its gradient is:

$$\frac{\partial f(M(t_0,\tau_k))}{\partial \tau_{ij}} = \frac{v^*_{\max}\left(\frac{\partial M(t_0,\tau_k)}{\partial \tau_{ij}}\right) u_{\max}}{v^*_{\max} u_{\max}}, \tag{10}$$

where $v_{\max}$ is the eigenvector associated with $\bar{\lambda}_{\max}$ of $M(t_0,\tau_k)^*$, satisfying $M(t_0,\tau_k)^* v_{\max} = \bar{\lambda}_{\max} v_{\max}$. Since $M(t_0,\tau_k)$ is real, $M(t_0,\tau_k)^* = M(t_0,\tau_k)^T$ and $M(t_0,\tau_k)^T v_{\max} = \lambda_{\max} v_{\max}$. By the Perron–Frobenius theorem (Lemma 1), the dominant eigenvector is real and positive, so $v^*_{\max} = v^T_{\max}$. Note that $v^T_{\max}$ and $u_{\max}$ are the left and right eigenvectors corresponding to $\lambda_{\max}$ of $M(t_0,\tau_k)$. Consequently, (10) simplifies to:

$$\frac{\partial f(M(t_0,\tau_k))}{\partial \tau_{ij}} = \frac{v^T_{\max}\left(\frac{\partial M(t_0,\tau_k)}{\partial \tau_{ij}}\right) u_{\max}}{v^T_{\max} u_{\max}}, \tag{11}$$

providing the gradient vector $\nabla f(M(t_0,\tau_k))$. This gradient is then used in the gradient descent step specified in (7).

Projection Step. The projection step in (7) minimizes $\|\tau - y_{k+1}\|_2^2$ subject to the constraint set of (6), resulting in linear constraints. This problem can be reformulated as a convex *Quadratic Programming (QP)* problem [35], allowing the optimal τ to be efficiently computed at each step.

Convergence Analysis. To analyze the convergence of the proposed algorithm to a stationary point and the operation of (7), we present the following lemmas.

Note that the spectral norm of the Hessian matrix $\nabla^2 f(\tau)$ is $|\lambda_{\max}(\nabla^2 f(\tau))|$ because the Hessian matrix of $f(\tau)$ is symmetric and real.

Lemma 3. *The eigenvalues of the matrix $M(t_0,\tau)$ (cf. (5)) are continuous functions of τ.*

Proof. This follows directly from the continuity of the roots of the characteristic polynomial of $M(t_0,\tau)$ [36]. □

Lemma 4. *The function $f(\tau) = \lambda_{\max}(M(t_0,\tau))$ is L-smooth.*

Proof. The set of all matrices $M(t_0,\tau)$ over possible travel rate matrices T (defined in Section II-B) is bounded and compact. By Thm. 1, $f(\tau)$ is ∞ times differentiable, so every element of its Hessian is continuous and differentiable. From the continuity of the Hessian and maximum eigenvalue (see Thm. 1) we have that the largest element of the Hessian achieves its maximum value on the compact set consisting of all $M(t_0,\tau)$ over all the possible travel rate matrices T. As a result, the spectral norm of the Hessian of $f(\tau)$ ($\|\nabla^2 f(x)\|_2$) is bounded and from [37] the maximum eigenvalue function $f(\tau)$ has a Lipschitz continuous gradient. □

After establishing that the dominant eigenvalue function $f(\tau)$ is L-smooth,we present the convergence result for the PGD operation with backtracking line search described in (7).

Theorem 2. *Let $f(\tau_k) = \lambda_{\max}(M(t_0,\tau_k))$. Executing the operation in (7), we have*

$$\lim_{k\to\infty} \nabla(f(\tau_k)) = 0. \tag{12}$$

Proof. Let $\{\tau_k\}$ be the sequence generated by (7). From the convergence of backtracking line search for differentiable and L-smooth functions [32], it follows that $\lim_{k\to\infty} \nabla(f(\tau_k)) = 0$. □

Theorem 2 establishes global convergence for the proposed PGD algorithm, independent of the initial point.

V. COVID-19 Model with Optimal Quarantine Rates

As another outbreak-controlling paradigm inspired by the optimization framework discussed earlier, this section extends the COVID-19 model in (1) by incorporating quarantine measures for infected individuals. Assigning an economic cost to each quarantined individual, we aim to optimize quarantine strategies to minimize the quarantined population while containing the infection spread.

A. Integrating Quarantining into a COVID-19 Model

The extended model introduces the following modifications:

1) Asymptomatic infected individuals x^{a}_i at each node i (a) exhibit automatic recovery at a rate of r^{a}, or (b) develop symptoms at a rate of ϵ, or (c) are quarantined with rate q^{a}_i, with k_i denoting the proportion of the quarantined population at node i.
2) Symptomatic cases x^{s}_i (a) experience automatic recovery at a rate of r^{s}, or (b) transition to a quarantined state at a rate of q^{s}_i.
3) Quarantined individuals k_i recover at a rate of r^q.

The resulting Susceptible-Infected-Quarantined-Recovered (SIQR) model is:

$$\dot{s}_i = -s_i \sum_{j=1}^{n} a_{ij}(\beta^{\mathrm{a}} x^{\mathrm{a}}_j + \beta^{\mathrm{s}} x^{\mathrm{s}}_j), \tag{13a}$$

$$\dot{x}^{\mathrm{a}}_i = s_i \sum_{j=1}^{n} a_{ij}(\beta^{\mathrm{a}} x^{\mathrm{a}}_j + \beta^{\mathrm{s}} x^{\mathrm{s}}_j) - (\epsilon + r^{\mathrm{a}} + q^{\mathrm{a}}_i) x^{\mathrm{a}}_i\ , \tag{13b}$$

$$\dot{x}^{\mathrm{s}}_i = \epsilon x^{\mathrm{a}}_i - (r^{\mathrm{s}} + q^{\mathrm{s}}_i) x^{\mathrm{s}}_i, \tag{13c}$$

$$\dot{k}_i = q^{\mathrm{a}}_i x^{\mathrm{a}}_i + q^{\mathrm{s}}_i x^{\mathrm{s}}_i - r^q k_i, \tag{13d}$$

$$\dot{h}_i = r^{\mathrm{a}} x^{\mathrm{a}}_i + r^{\mathrm{s}} x^{\mathrm{s}}_i + r^q k_i, \tag{13e}$$

The SIQR model retains the notation of (1) and incorporates quarantining for both asymptomatic and symptomatic individuals, who recover at a rate r^q.

B. Problem Formulation for Minimizing Quarantine Rates

Let $q^{\mathrm{a}} = (q^{\mathrm{a}}_1, \ldots, q^{\mathrm{a}}_n)$, $q^{\mathrm{s}} = (q^{\mathrm{s}}_1, \ldots, q^{\mathrm{s}}_n)$, and $q = (q^{\mathrm{a}}, q^{\mathrm{s}})$ represent the column vectors of quarantine rates. To analyze the disease-free equilibrium, we decouple the dynamics of $\dot{x}$ from (13) and focus on the $2n \times 2n$ sub-matrix $M(t,q)$:

$$M(t,q) = \begin{pmatrix} E & \beta^{\mathrm{s}} \operatorname{diag}(s(t)) A \\ \epsilon I & -(r^{\mathrm{s}} I + \operatorname{diag}(q^{\mathrm{s}})) \end{pmatrix}, \tag{14}$$

where $E = \beta^{\mathrm{a}} \operatorname{diag}(s(t)) A - (\epsilon + r^{\mathrm{a}}) I - \operatorname{diag}(q^{\mathrm{a}})$. The objective is to minimize quarantine rates $q^{\mathrm{s}}_i, q^{\mathrm{a}}_i$ to control infection spread and reduce economic costs within the network. These

rates can be assumed to be nonnegative. We note also that there is an upper bound on what these rates could plausibly be, since the *inverse* of these rates represents the time a typical individual would spend before being quarantined under a scenario where individuals do not transition between classes (e.g., symptomatic, asymptomatic, recovered). Consequently, we may assume without loss of generality a bound of 1 on all quarantine rates. To achieve this, we formulate the following optimization problem:

$$\begin{aligned} \min_q \quad & \sum_{i=1}^{n} \frac{z_i^a}{1-q_i^{\mathrm{a}}} + \frac{z_i^s}{1-q_i^{\mathrm{s}}} \\ \text{s.t.} \quad & \lambda_{\max}(M(t_0, q)) \leq -\alpha, \\ & \mathbf{0} \leq q \leq \mathbf{1}, \end{aligned} \tag{15}$$

where $z^a = (z_1^a, \ldots, z_n^a)$ and $z^s = (z_1^s, \ldots, z_n^s)$ represent the relative economic costs associated with quarantining asymptomatic and symptomatic cases at each node, respectively. The objective function in (15) aims to minimize the total economic cost of quarantine rates across all nodes. This formulation accounts for the challenges in identifying and quarantining asymptomatic individuals by incorporating random testing strategies. The potentially higher costs associated with detecting and quarantining asymptomatic carriers are reflected in the cost parameters z^{a}. The economic cost for each node increases nonlinearly with quarantine rates, modeling the growing logistical complexity and resource requirements associated with quarantining a larger fraction of the population. The summation aggregates these costs over all nodes, and the optimization seeks quarantine rates q that minimize this combined cost. The constraints ensure that the maximum eigenvalue of $M(t_0, q)$ is bounded by $-\alpha$, enforcing a condition for controlling infection spread (see Proposition 1). The upper bounds on both q^{a} and q^{s} allow for adjusting quarantine rates based on available resources and testing capabilities, acknowledging the practical limitations in selective quarantining. Consequently, the optimization problem balances minimizing quarantine-associated costs with achieving a decay rate of $-\alpha$ for infected cases.

C. Proposed Solution

The optimization method for solving problem (15) differs from our previous PGD-based approach for travel rates due to the nonlinear constraints involved. Unlike the linear constraints in problem (6), problem (15) introduces nonlinear constraints on quarantine rates, requiring an alternative approach.

Reduction of the Optimization Problem to Weight-Balancing. We now demonstrate that problem (15) can be reduced to a matrix balancing problem. This reduction relies on Assumption 1, which is typically satisfied by epidemic model parameters, as verified using Massachusetts data. In practice, the matrix balancing algorithm successfully solves problem (15) under these conditions.

Assumption 1. *Consider the matrix B_0:*

$$B_0 = \begin{pmatrix} \beta^{\mathrm{a}} \operatorname{diag}(s(t_0))A - (\epsilon + r^{\mathrm{a}} + 1)I & \beta^{\mathrm{s}} \operatorname{diag}(s(t_0))A \\ \epsilon I & -(r^{\mathrm{s}} + 1)I \end{pmatrix}$$

Let m be the largest absolute value of any diagonal element of B_0. Defining $x = \min_j(\epsilon\beta^{\mathrm{s}} s_j(t_0)A_{jj})$, we assume:

$$1 + \frac{x}{m^2} \geq m.$$

Assumption 1 is needed to ensure the solution is nonnegative. Now, we present the main theorem of our study:

Theorem 3. *The minimum quarantining problem in (15) can be reduced to a matrix balancing problem provided that the Assumption 1 is satisfied, the infection flow matrix A (from Sec. II-B) is strongly connected, $s(t_0) > 0$, and the problem is feasible.*

Proof. See Appendix A. □

Inspired by [15], we reduced problem (15) to a matrix balancing problem, which is known to have polynomial complexity with respect to the number of unknown variables ($2n$). Problem (15) is inherently complex due to the eigenvalue condition in its first constraint, which can potentially lead to higher-order computational complexity. Although the matrix balancing approach requires inverting a $2n \times 2n$ matrix B_0—an operation with cubic complexity—our proposed solution remains polynomial in terms of the number of parameters ($2n$).

Remark 2. *Problems (6) and (15) can be reformulated as Geometric Programs (GPs). For (6), this would still require GD in a transformed space, complicating analysis. For (15), while matrix scaling is formulated as a GP in [38], the presented complexity analysis has not proved to be competitive. Thus, our proposed solutions generally outperform GP formulations in terms of efficiency and speed.*

Connection of Constraints with the Epidemic Basic Reproduction Number. In epidemiological analysis, the reproduction number R_0 is a key metric, as it indicates whether a disease outbreak will escalate or dissipate naturally. Unfortunately, calculating R_0 is often non-trivial due to the lack of comprehensive data. Motivated by this, we establish a relationship between the constraint $\lambda_{\max}(M(t_0)) \leq -\alpha$ and the epidemic's reproduction number R_0. This connection is crucial, as modifying our constraints can prevent an epidemic from escalating into a pandemic or spreading extensively within a population.

Theorem 4. *The set $R_0 \leq 1$ is equivalent to $\lambda_{\max} \leq 0$.*

Proof. See Appendix B. □

Theorem 4 implies that imposing the condition $\lambda_{\max}(M(t_0)) \leq -\alpha$ provides a set of solutions that enforces a bound on the disease reproduction number $R_0 \leq r$, for $r \in [0, 1]$.

While matrix balancing is our primary method—yielding a closed-form solution as shown in Appendix A, we now present a complementary approach via augmented primal-dual gradient dynamics to demonstrate semi-global exponential convergence under an alternative set of conditions.

Convergence via Augmented Primal-Dual Gradient Dynamics for Optimal Quarantine Control. We now extend our approach to solving the optimal quarantine problem by

applying the augmented primal-dual gradient dynamics (Aug-PDGD). This extension demonstrates semi-global exponential convergence to a KKT point of the problem. The following propositions and theorems collectively establish this result.

Proposition 2. *Assuming the feasibility of (15), the cost function, defined as* $f(q) = \sum_{i=1}^{n} \left(\frac{z_i^a}{1-q_i^a} + \frac{z_i^s}{1-q_i^s} \right)$*, is continuously differentiable and strongly convex on the feasible domain* $\mathbf{0} \leq q < \mathbf{1}$*. Moreover,* $M(t_0, q)$ *can be expressed as the sum of an essentially nonnegative matrix and a diagonal matrix with the elements of the vector* $-q$ *on its diagonal. Therefore, as demonstrated in [39], the dominant eigenvalue of the matrix* $M(t_0, q)$ *is convex. Defining* $g_1(q) = \lambda_{\max}(M(t_0, q)) + \alpha$*,* $g_{(1+i)} = -q_i$*, and* $g_{2n+1+i} = q_i - 1$ *for all* $i \in \{1, \ldots, 2n\}$*,* $g(q)$ *is continuously differentiable and convex.*

Given Proposition 2, we are now ready to analyze the augmented primal-dual gradient dynamics. We introduce the augmented Lagrangian of (15) formulated as [40]

$$L_\rho(q, \lambda) = f(q) + \Theta_\rho(q, \lambda), \qquad \lambda \geq \mathbf{0}, \tag{16}$$

where

$$\Theta_\rho(q, \lambda) := \sum_{i=1}^{4n+1} \frac{[\rho g_i(q) + \lambda_i]_+^2 - \lambda_i^2}{2\rho}.$$

The augmented primal-dual gradient dynamics are given by

$$\dot{q}(t) = -\nabla f(q(t)) - \sum_{i=1}^{4n+1} [\rho g_i(q(t)) + \lambda_i(t)]_+ \nabla g_i(q(t)) \tag{17a}$$

$$\dot{\lambda}(t) = \sum_{i=1}^{4n+1} \frac{[\rho g_i(q) + \lambda_i(t)]_+ - \lambda_i(t)}{\rho} e_i. \tag{17b}$$

We now establish the Lipschitz smoothness of the cost function and the constraints in the following theorems.

Theorem 5. *Given* $g_1(q) = \lambda_{\max}(M(t_0, q)) + \alpha$*, (11) and (14) imply that*

$$\nabla g_1(q) = \frac{v_{\max} \circ u_{\max}}{v_{\max}^T u_{\max}}.$$

Recall that $v_{\max}^T$ *and* $u_{\max}$ *represent the left and right eigenvectors associated with* $\lambda_{\max}(M(t_0, q))$*. Hence,* $\|\nabla g_1(q)\| \leq L_{g,1}$ *(see Appendix C for proof), and* $g_1(q)$ *is also* $M_{g,1}$*-smooth (see Lemma 4). Additionally, for all* $i \geq 2$*, the gradients* ∇g_i *are Lipschitz continuous and have bounded norms, which is evident from their definitions.*

Proposition 3 ([40])**.** *Denoting* $y(t) = (q(t), \lambda(t))$*,* $t \geq 0$ *as a differentiable trajectory satisfying (17). Then, for a KKT point of (16),* $y^* = (q^*, \lambda^*)$*, we have* $\|y(t) - y^*\| \leq \|y(0) - y^*\|$*, for all* $t \geq 0$*.*

With bounded trajectories established, we have the following theorem.

Theorem 6. *The gradient of the cost function* $f(q)$ *is Lipschitz continuous over the region traversed by the primal gradient dynamics described by (17).*

Proof. See Appendix D. □

We now verify that the *Linear Independence Constraint Qualification (LICQ)* holds at q^* in Proposition 4.

Proposition 4. *Let the active set at the local optimal solution* q^* *be denoted by* $\mathcal{I} := \{i : g_i(q^*) = 0\}$*. Therefore,* q^* *is a regular local minimum, i.e.,* $\nabla g_i(q^*)$ *for* $i \in \mathcal{I}$ *are linearly independent.*

Proof. See Appendix E. □

Combining convexity, Lipschitz, and regularity conditions, Corollary 1 establishes semi-global exponential stability of the Aug-PDGD at the KKT point.

Corollary 1. *Under Propositions 2 and 4, and Theorems 5 and 6, the application of augmented primal-dual gradient dynamics (Aug-PDGD) to (15) achieves semi-global exponential stability. Specifically, the KKT point* $y^* = (q^*, \lambda^*)$ *is a semi-globally exponentially stable equilibrium of the Aug-PDGD.*

This result follows immediately from Theorem 6, Proposition 4 and the results of [40], which examine the stability of Aug-PDGD for smooth convex optimization problems with general convex and nonlinear inequality constraints. Consequently, the distance to the optimal solution decays exponentially from any initial point, although the convergence rate may depend on the initial distance to a stationary point.

It should be noted that [40] assumes the Lipschitz continuity of $\nabla f(q)$. However, as stated in Theorem 6, what is actually required is the Lipschitz continuity of $\nabla f(q)$ over the region invariant under the primal gradient dynamics.

VI. Simulation Results

In this section, we present simulation results for our optimization strategies. For problems **P1** and **P2**, we consider a 14-node network representing the counties of Massachusetts to demonstrate the applicability and advantages of our approaches in real world scenarios.

A. Model Parameters

Massachusetts 14-Node Network. The network consists of 14 nodes, each representing a Massachusetts county. Population data ($N_i, i \in \{1, ..., 14\}$) is sourced from the 2020 Census [41], while travel rates (τ) for the infection flow matrix (A) are derived from the Human Mobility Flow dataset [26] following Section II-B. We assume $t_i = \frac{1}{3}$, representing one-third of the time spent outside.

Epidemic and Economic Parameters. County-level GDP data from the Bureau of Economic Analysis [42] is used to compute economic losses $(z_i^{\mathrm{a}}, z_i^{\mathrm{s}})$ as $z_i^{\mathrm{a}} = z_i^{\mathrm{s}} = g_i / g_{\max}$, where g_i is the GDP of county i, and $g_{\max}$ is the highest GDP across all counties. Epidemic parameters are taken from [17], [18], with recovery rates ($r^a = r^s = r^q = \gamma = 0.2$), symptom development rate ($\epsilon = 0.32$), and transmission rates (β^a, β^s). Following [15], $\beta^a = \eta\beta^s$ with $\eta = 0.6754$, and β^s is adjusted to match observed growth rates. Adjustments to β ensure A aligns with the required growth rate.

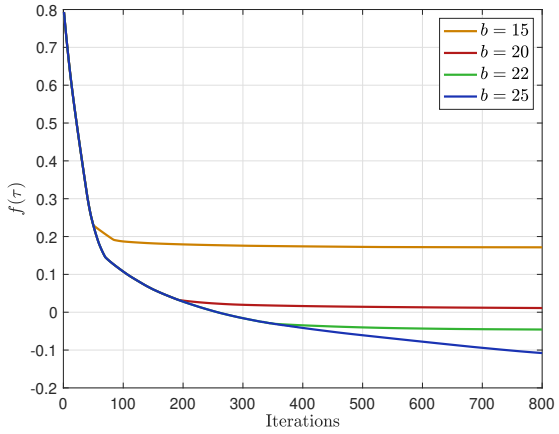

Fig. 1. Optimal $f(\tau)$ values in problem (6) for various budgets b, as travel rates τ change via (7).

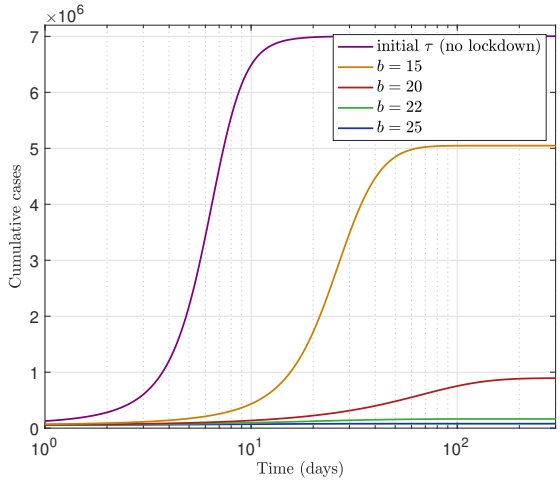

Fig. 2. Cumulative cases (infected, quarantined, recovered) under varying travel rate constraints in Massachusetts.

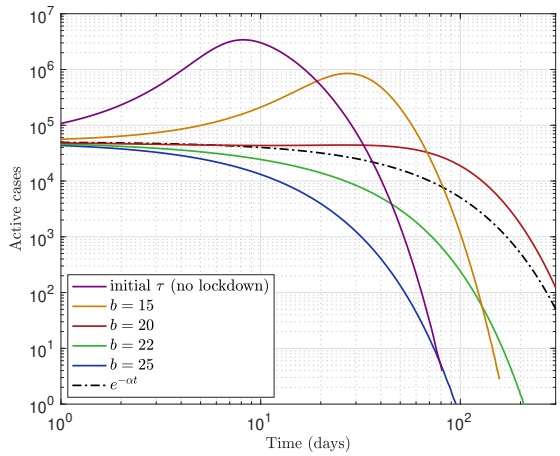

Fig. 3. Active cases (asymptomatic and symptomatic) with different travel rate constraints in Massachusetts.

Initial Rates. Initial susceptible rates ($s(t_0)$) are calculated using cumulative case data [43] adjusted for underreporting by dividing cumulative cases by 0.14 [18], [44]. For node i, $s_i(t_0) = 1 - c_i(t_0)/(0.14N_i)$, where $c_i(t_0)$ is the cumulative cases. April 1, 2020, is used as the initial state (t_0). Recovered cases are estimated using the U.S. recovery ratio on April 1, 2020 ($\frac{8878}{215215}$ [15]), scaled by node-level cumulative infected cases plus deaths. Active cases (symptomatic: 14%, asymptomatic: 86%) are adjusted by 0.14 to account for underreporting.

B. Massachusetts County-Level 14 Node Network

Optimizing Travel Rates. We validate the optimal solution for (6) over the Massachusetts 14-node network.

Figure 1 displays $f(\tau) = \lambda_{\max}\big(M(t_0, \tau)\big)$ (cf. (6)) computed via the PGD algorithm. For each budget b, the algorithm converges to a local optimum τ^*. As b increases, the optimal travel rates diverge from the uncontrolled values, minimizing $f(\tau)$ and lowering $\lambda_{\max}\big(M(t_0, \tau^*)\big)$ for larger b. Specifically, when $b > 20$, $f(\tau^*) < 0$, so the epidemic converges faster to a disease-free equilibrium. The degree of restrictions (quantified by b) mainly affects travel rates, necessitating network-specific customization.

Figure 2 shows the cumulative number of infected and recovered cases using the optimal travel rates from the PGD algorithm. As expected, larger b—implying stricter lockdown measures—results in fewer cumulative cases and faster epidemic control. Similarly, Fig. 3 illustrates the number of active infected cases for these optimal travel rates. Notably, for $b > 20$, we achieve a reduction rate of $-\alpha = -0.0231$, corresponding to halving active cases every 30 days.

Optimizing Quarantine Rates. Figures 4 and 5 compare our optimal quarantining rates with various policies. In *uniform quarantining*, all locations share identical rates chosen so that the total economic cost matches that of the optimal policy. In *random quarantining*, rates are drawn uniformly at random, scaled to equal the our optimal policy's cost. In a *uniformly bounded decline policy*, rates are set to keep each node's infection decay rate within a bound, again matching the optimal economic cost. For the same economic expenditures, our optimal quarantine rates minimize both cumulative and active infections across the network.

Given that (6) and (15) can be solved efficiently, we can periodically re-optimize the travel rates or quarantine measures based on the current epidemic state. This would impose stricter rules initially when susceptible rates are higher, gradually relaxing restrictions as the susceptible population decreases. This approach maintains the benefits of adaptability while avoiding premature relaxation of control measures, aligning with the practical reality that policy changes require implementation time.

VII. Conclusions

In this paper, we presented a framework for epidemic control with two approaches. The first focuses on strategically reducing travel rates to contain the virus, utilizing the maximum eigenvalue function and the PGD algorithm for optimization. The second enhances the SIR model with a quarantine strategy to minimize costs and decrease new infections rapidly through node-specific rates. We propose a solution that simplifies optimal quarantining into a weight-balancing problem and establish a link between optimization constraints and the

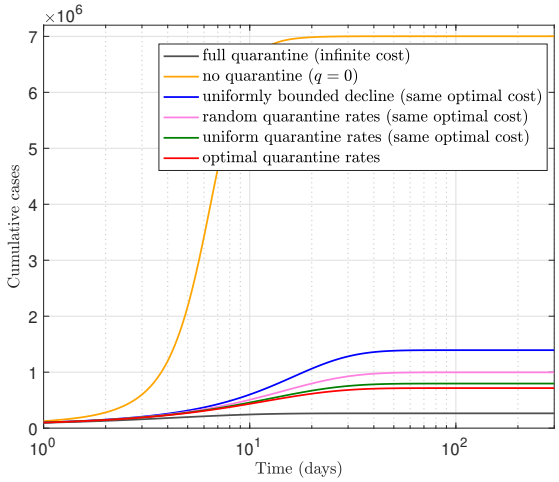

Fig. 4. Cumulative cases (infected, quarantined, recovered) for different quarantine rates in Massachusetts. For the optimal policy, $\alpha = 0.023$, halving infections every 30 days.

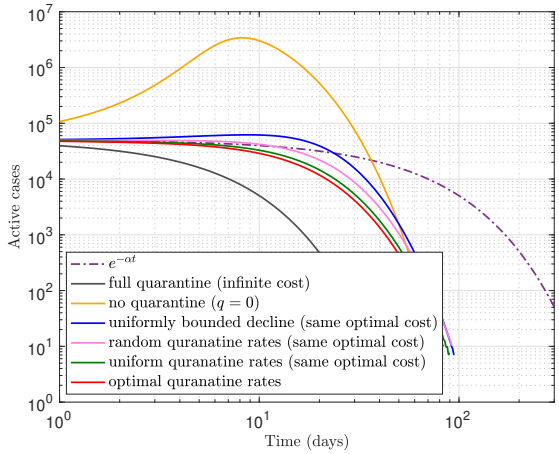

Fig. 5. Active cases (asymptomatic and symptomatic) for various quarantine policies in Massachusetts. For the optimal policy, $\alpha = 0.023$, halving infections every 30 days.

epidemic's basic reproduction number. Finally, applying (Aug-PDGD) to our optimal quarantine problem ensures exponential stability of the solution.

Our numerical results highlight the efficiency of both approaches in controlling the epidemic. Although we constructed the network within the county-level framework, it's noteworthy that, given data availability, these methods can be applied to much smaller nodes (e.g., zip code or census track levels).

Appendix A
Proof of Theorem 3

Consider the problem formulation in (15). Setting $w = \mathbf{1} - q$, we equivalently have

$$\begin{aligned} \min_w \quad & \sum_{i=1}^{n} \frac{z_i^{\mathrm{a}}}{w_i^{\mathrm{a}}} + \frac{z_i^{s}}{w_i^{\mathrm{s}}} \\ \text{s.t.} \quad & \lambda_{\max}(A_0) \le 0 \ , \\ & \mathbf{0} \le w \le \mathbf{1} \ , \end{aligned} \tag{18}$$

where from (14)

$$A_0 = \begin{pmatrix} \operatorname{diag}(w^{\mathrm{a}}) + E' & \beta^{\mathrm{s}} \operatorname{diag}(s(t_0))A \\ \epsilon I & \operatorname{diag}(w^{\mathrm{s}}) - (r^{\mathrm{s}} + 1 - \alpha)I \end{pmatrix},$$

and $E' = \beta^{\mathrm{a}} \operatorname{diag}(s(t_0))A - (\epsilon + r^{\mathrm{a}} + 1 - \alpha)I$.

We now find the range of α ensuring there exists a nonnegative w satisfying the maximum eigenvalue constraint in (18). First assume

$$\alpha < \min(r^{s}+1,\ \epsilon + r^{a} + 1 - \max_i (\beta^{\mathrm{a}} \operatorname{diag}(s(t_0))A)_{ii}), \tag{19}$$

where $\max_i (\beta^{\mathrm{a}} \operatorname{diag}(s(t_0))A)_{ii}$ is the maximum diagonal element of $\beta^{\mathrm{a}} \operatorname{diag}(s(t_0))A$, which is known and fixed. If (19) does not hold, then matrix A_0 cannot be continuous time stable (the first constraint in (18) fails for any w). In particular, when (19) is not satisfied, no $d > \mathbf{0}$ can fulfill $A_0 d \le \mathbf{0}$, regardless of w (see the first bullet of Lemma (2)).

Let us write

$$\begin{aligned} A_0 &= \operatorname{diag}(w) + \begin{pmatrix} E' & \beta^{\mathrm{s}} \operatorname{diag}(s(t_0))A \\ \epsilon I & -(r^{\mathrm{s}} + 1 - \alpha)I \end{pmatrix} \\ &= \operatorname{diag}(w) + B_0, \end{aligned} \tag{20}$$

where $w = (w^{\mathrm{a}}, w^{\mathrm{s}}) \in \mathbb{R}^{2n}$, and $E' = \beta^{\mathrm{a}} \operatorname{diag}(s(t_0))A - (\epsilon + r^{\mathrm{a}} + 1 - \alpha)I$. By the Perron-Frobenius theorem, adding the nonnegative diagonal $\operatorname{diag}(w)$ cannot decrease the largest eigenvalue of B_0. Thus, for (18) to be feasible, B_0 must be Hurwitz. Condition (19) is necessary but may not be sufficient for B_0 to be Hurwitz. To address that, write

$$\begin{aligned} B_0 = &\begin{pmatrix} \beta^{\mathrm{a}} \operatorname{diag}(s(t_0))A - (\epsilon + r^{\mathrm{a}} + 1)I & \beta^{\mathrm{s}} \operatorname{diag}(s(t_0))A \\ \epsilon I & -(r^{\mathrm{s}} + 1)I \end{pmatrix} \\ &+ \alpha I = C_0 + \alpha I. \end{aligned}$$

So C_0 must be Hurwitz, and α must be chosen such that adding αI does not does not destabilize C_0. Hence, $\alpha < -\lambda_{\max}(C_0)$ is required for feasibility.

Since B_0 is Hurwitz, B_0 is invertible and $-B_0^{-1} \ge \mathbf{0}$ ([45, Thm. 10.3]). By Lemma 2, A_0 is continuous-time stable if and only if $-B_0^{-1} \operatorname{diag}(w)$ is discrete-time stable. Since changing the order of the product of two matrices does not affect the eigenvalues of the product, equivalently $\operatorname{diag}(w)(-B_0^{-1})$ must be discrete-time stable. By part (3) of Lemma 2, this holds if and only if $-B_0^{-1} - \operatorname{diag}(w)^{-1}$ is continuous-time stable.

For nonnegative w, let $v_i = {w_i}^{-1}$. Then (18), ignoring $w \le \mathbf{1}$, is equivalent to

$$\begin{aligned} \min_v \quad & z^T v \\ \text{s. t.} \quad & \lambda_{\max}(-B_0^{-1} - \operatorname{diag}(v)) \le 0, \\ & v \ge \mathbf{0} \end{aligned} \tag{21}$$

where $-B_0^{-1}$ is Metzler. Due to the strong connectivity of A, the two upper blocks in B_0 are strongly connected, and its two lower diagonal blocks ensure B_0 is also strongly connected. Hence, $-B_0$ is irreducible, so $-B_0^{-1}$ is also irreducible. The objective in (21) is to find v^* minimizing $z^T v^*$ such that $-B_0^{-1} - \operatorname{diag}(v^*)$ is Hurwitz. By [16, Theorem 3], this reduces to a matrix balancing problem. Specifically, let $d^* \in \mathcal{R}^{2n}_{>0}$ be such that

$$(\operatorname{diag}(d^*))^{-1} \operatorname{diag}(z)(-B_0^{-1}) \operatorname{diag}(d^*)$$

is weight balanced. Then (21) has a unique optimum

$$v^* = (\operatorname{diag}(d^*))^{-1}(-B_0^{-1})\operatorname{diag}(d^*)\mathbf{1} \ . \tag{22}$$

Hence, (18) is equivalent to a matrix balancing problem for $w \geq \mathbf{0}$, or equivalently $q \leq \mathbf{1}$.

To finalize, we also require $w \leq \mathbf{1}$ (equivalently $q \geq \mathbf{0}$). Let us see the solution v^* in more detail. As discussed previously, B_0 is a Hurwitz matrix with nonnegative off-diagonal elements and negative diagonal elements. Suppose m is the absolute value of the most negative diagonal element of B_0, or

$$m = \max_i |(B_0)_{ii}| > 0 \ .$$

Let us write $B_0 = B - mI$, where B is a nonnegative matrix. From the Perron-Frobenius theorem, we have $\rho(B) > 0$ and $\rho(B) - m$ is an eigenvalue of the Hurwitz matrix B_0.

$$\begin{aligned} B_0^{-1} &= (B - mI)^{-1} = \frac{1}{m}(\frac{1}{m}B - I)^{-1} \\ &= -\frac{1}{m}\sum_{n=0}^{\infty}\left(\frac{1}{m}B\right)^n = -\frac{1}{m}\sum_{n=0}^{\infty}\left(I + \frac{1}{m}B_0\right)^n \ . \end{aligned} \tag{23}$$

By substituting (23) in (22), v^* can be derived as

$$v^* = \frac{1}{m}(\operatorname{diag}(d^*))^{-1}\sum_{n=0}^{\infty}\left(I + \frac{1}{m}B_0\right)^n \operatorname{diag}(d^*)\mathbf{1} \ . \tag{24}$$

Thus, to have $w \leq \mathbf{1}$, we require $v^* \geq \mathbf{1}$ or equivalently, the sum of row elements of

$$(\operatorname{diag}(d^*))^{-1}\sum_{n=0}^{\infty}\left(I + \frac{1}{m}B_0\right)^n \operatorname{diag}(d^*)$$

should be greater or equal to m. Indeed, defining $\sum_{n=0}^{\infty}\left(I + \frac{1}{m}B_0\right)^n = Q$, we need

$$\sum_{j=1}^{2n}\frac{d_j^*}{d_i^*}Q_{ij} \geq m \qquad \forall i \in \{1, 2, \ldots, 2n\} \ . \tag{25}$$

Notice that $\frac{1}{m}B_0$ is a matrix with nonnegative off-diagonal elements and negative diagonal elements of $-1 \leq \frac{(B_0)_{ii}}{m} < 0$. Thus, $(I + \frac{1}{m}B_0)$ is a nonnegative matrix with diagonal elements, and

$$0 \leq (I + \frac{1}{m}B_0)_{ii} < 1 \ .$$

Hence,

$$Q \geq I + [I + \frac{1}{m}B_0] + [(I + \frac{1}{m}B_0)^2] = \bar{Q} \tag{26}$$

Letting $(I + \frac{1}{m}B_0)_{ii} = 0$, we have

$$(I + \frac{1}{m}B_0) \geq \begin{pmatrix} \frac{1}{m}\tilde{A} & \frac{\beta^{\mathrm{s}}}{m}\operatorname{diag}(s(t_0))A \\ \frac{\epsilon}{m}I & \mathbf{0} \end{pmatrix} \ , \tag{27}$$

where $\tilde{A} = \beta^{\mathrm{a}}\operatorname{diag}(s(t_0))A$ that its diagonal elements are replaced with zero. Substituting (27) into (26), we derive a lower bound of $\bar{Q}$ as $\tilde{Q}$:

$$\tilde{Q} = \begin{pmatrix} \tilde{Q}_{11} & \tilde{Q}_{12} \\ \frac{\epsilon}{m}I + \frac{\epsilon}{m^2}\tilde{A} & I + \frac{\epsilon\beta^{\mathrm{s}}}{m^2}\operatorname{diag}(s(t_0))A \end{pmatrix}, \tag{28}$$

where

$$\tilde{Q}_{11} = I + \frac{\tilde{A}}{m} + \frac{1}{m^2}(\tilde{A}^2 + \epsilon\beta^{\mathrm{s}}\operatorname{diag}(s(t_0))A),$$

$$\tilde{Q}_{12} = \frac{\beta^{\mathrm{s}}}{m}\operatorname{diag}(s(t_0))A + \frac{\beta^{\mathrm{s}}}{m^2}\tilde{A}\operatorname{diag}(s(t_0))A \ .$$

From the definition of B_0 in (20), m can be written as

$$\begin{aligned} m = \max\Big(&r^s + 1 - \alpha, \\ &\epsilon + r^a + 1 - \alpha - \min(\beta^{\mathrm{a}}\operatorname{diag}(s(t_0))A)_{ii}\Big) \ . \end{aligned}$$

Substituting Assumption 1 into the definition of $\tilde{Q}$, we have

$$\begin{aligned} \tilde{Q}_{ii} &= 1 + \frac{1}{m^2}((\tilde{A}^2)_{jj} + \epsilon\beta^{\mathrm{s}}s_i(t_0)A_{jj}) \\ &\geq 1 + \frac{\epsilon}{m^2}\beta^{\mathrm{s}}s_i(t_0)A_{jj} \geq 1 + \frac{x}{m^2} \\ &\geq m \ , \qquad i \in \{1, \ldots, n\} \ , \end{aligned}$$

and

$$\begin{aligned} \tilde{Q}_{ii} &= 1 + \frac{1}{m^2}\epsilon\beta^{\mathrm{s}}s_j(t_0)A_{jj} \geq 1 + \frac{x}{m^2} \geq m \\ &\geq m \ , \qquad i \in \{n+1, \ldots, 2n\} \ . \end{aligned}$$

Finally,

$$\sum_{j=1}^{2n}\frac{d_j^*}{d_i^*}Q_{ij} \geq Q_{ii} \geq \bar{Q}_{ii} \geq \tilde{Q}_{ii} \geq m \ , \tag{29}$$

for all $i \in \{1, 2, \ldots, 2n\}$. Hence, $v^* \geq \mathbf{1}$, and equivalently $q^* \geq \mathbf{0}$. Subsequently, substituting the definitions of v and w, the optimal quarantined rates are calculated as

$$q^* = \mathbf{1} + 1./\left((\operatorname{diag}(d^*))^{-1}B_0^{-1}(\operatorname{diag}(d^*))\mathbf{1}\right) \ .$$

Appendix B
Proof of Theorem 4

We will establish that initiating from $R_0 < 1$ leads us to $\lambda_{\max}(M(t_0)) \leq 0$. Assume

$$R_0 \leq 1 \ .$$

We have

$$M(t_0) = \begin{pmatrix} E & \beta^{\mathrm{s}}\operatorname{diag}(s(t_0))A \\ \epsilon I & -(r^{\mathrm{s}} + \operatorname{diag}(q^{\mathrm{s}}))I \end{pmatrix},$$

where $E = \beta^{\mathrm{a}}\operatorname{diag}(s(t_0))A - (\epsilon + r^{\mathrm{a}} + \operatorname{diag}(q^{\mathrm{a}}))I$. Let us write $M(t_0)$ as

$$M(t_0) = F + V,$$

where

$$F = \begin{pmatrix} \beta^{\mathrm{a}}\operatorname{diag}(s(t_0))A & \beta^{\mathrm{s}}\operatorname{diag}(s(t_0))A \\ \mathbf{0} & \mathbf{0} \end{pmatrix},$$

and

$$V = \begin{pmatrix} -(\epsilon + r^{\mathrm{a}})I - \operatorname{diag}(q^{\mathrm{a}})) & \mathbf{0} \\ \epsilon I & -(r^{\mathrm{s}} + \operatorname{diag}(q^{\mathrm{s}}))I \end{pmatrix}.$$

Note that F is nonnegative and V is Metzler and Hurwitz. Using the definition of R_0 in [12, Definition 1] we have

$$R_0 = \rho(FV^{-1}) = \rho(-FV^{-1}) \leq 1. \tag{30}$$

Utilizing the early results of Thm. 3, (30) is equivalent with

$$\lambda_{\max}(F + V) \leq 0,$$

(i.e., $F + V$ is Hurwitz). Hence, we have

$$\lambda_{\max}(M(t_0)) = \lambda_{\max}(F + V) \leq 0.$$

Therefore, the set $\lambda_{\max}(M(t_0)) \leq 0$ is equivalent with the set $R_0 \leq 1$.

APPENDIX C

We argue that $\left\| \frac{v_{\max} \circ u_{\max}}{v_{\max}^T u_{\max}} \right\|$ is bounded for any choice of $M(t_0, q)$. Without loss of generality, we may assume the left and right eigenvectors are normalized to have unit norm. In that case, the norm of the numerator is automatically bounded.

Applying Lemma 1 to $M(t_0, q)$ and $M(t_0, q)^T$, we have that $u_{\max}$ and $v_{\max}$ are positive as are the respective dominant eigenvectors. Hence, the dot product of the corresponding Perron-Frobenius left and right eigenvectors is always positive. This also implies that the denominator is bounded away from zero, for otherwise by compactness we could find a matrix M such that $v_{\max}^T u_{\max} = 0$, contradicting positivity of these vectors. Therefore, $\|\nabla g_1(q)\|$ is bounded.

APPENDIX D
PROOF OF THEOREM 6

It is obvious that the gradient of $f(q)$ is Lipschitz as long as every $q_i(0)$ is bounded away from 1. We thus need to argue that the primal-dual dynamics keep all $q_i(0)$ uniformly bounded away from one.

We start by expressing the primal dynamics as given by (17a):

$$\dot{q}(t) = -\nabla f(q(t)) - \sum_{i=1}^{4n+1} [\rho g_i(q(t)) + \lambda_i(t)]_+ \nabla g_i(q(t)). \quad (31)$$

Here, $\lambda(t) \in \mathbb{R}_{\geq 0}^{(4n+1)}$ is a vector that remains in a compact region of space for all $t \geq 0$ by Proposition 3. Therefore, using (5), we can state that the second part of (31) is bounded.

Note that as $q_i \to 1$, we have $|\nabla_i f(q(0))|$ approaches ∞, and $\dot{q}_i < 0$. This immediately implies there is some $q' < 1$ such that the region $[0, q']^n$ remains invariant under the differential equation (31). Remaining within this region implies the Lipschitz continuity of $\nabla f(q)$.

APPENDIX E
PROOF OF PROPOSITION 4

Suppose q^* is a local minimum of (15). Therefore, $q_i^* \neq 1$ for all $i \in \{1, 2, \ldots, 2n\}$. This implies the active set is

$$\mathcal{I} = \{j : g_j(q^*) = 0,\ j \in J\}\ ,$$

where $J = \{1, 2, \ldots, 2n+1\}$.

First, assume $\mathcal{I} \neq J$. From the definition provided for g_1, $\nabla g_1 = \frac{v_{\max} \circ u_{\max}}{v_{\max}^T u_{\max}}$ is an element-wise positive vector by the same analysis provided in Appendix D. It is therefore evident that any $2n$ vectors of g_j, for all $j \in J$, would have linearly independent gradients at any point q^*.

Now, consider $\mathcal{I} = J$. This implies $q^* = \mathbf{0}$. However, for our model of the outbreak in (15), setting all quarantine rates equal to zero implies having no interventions. Hence, the constraint function $g_1 = \lambda_{\max}(M(t_0, q = \mathbf{0})) + \alpha$ would not be active. Hence, $\mathcal{I}$ cannot include all $j \in J$, and this proves the non-linearity of the active set at any local minimum q^*.

REFERENCES

[1] J. Center, "Covid-19 dashboard," *Johns Hopkins University*, 2021.

[2] A. Linde, M. Rotzén-Östlund, B. Zweygberg-Wirgart, S. Rubinova, and M. Brytting, "Does viral interference affect spread of influenza?" *Eurosurveillance*, vol. 14, no. 40, p. 19354, 2009.

[3] C. Nowzari, V. M. Preciado, and G. J. Pappas, "Analysis and control of epidemics: A survey of spreading processes on complex networks," *IEEE Control Systems Magazine*, vol. 36, no. 1, pp. 26–46, 2016.

[4] P. E. Paré, C. L. Beck, and T. Başar, "Modeling, estimation, and analysis of epidemics over networks: An overview," *Annual Reviews in Control*, vol. 50, pp. 345–360, 2020.

[5] S. Lee, G. Chowell, and C. Castillo-Chávez, "Optimal control for pandemic influenza: The role of limited antiviral treatment and isolation," *Journal of Theoretical Biology*, vol. 265, no. 2, pp. 136–150, 2010.

[6] M. Hayhoe, F. Barreras, and V. M. Preciado, "Multitask learning and nonlinear optimal control of the covid-19 outbreak: A geometric programming approach," *Annual Reviews in Control*, vol. 52, pp. 495–507, 2021.

[7] A. Khanafer and T. Basar, "An optimal control problem over infected networks," in *Proceedings of the International Conference of Control, Dynamic Systems, and Robotics*, vol. 125, 2014, pp. 1–6.

[8] F. Liu and M. Buss, "Optimal control for heterogeneous node-based information epidemics over social networks," *IEEE Transactions on Control of Network Systems*, vol. 7, no. 3, pp. 1115–1126, 2020.

[9] Y. Yi, L. Shan, P. E. Paré, and K. H. Johansson, "Edge deletion algorithms for minimizing spread in sir epidemic models," *SIAM Journal on Control and Optimization*, vol. 60, no. 2, pp. S246–S273, 2022.

[10] A. R. Hota, J. Godbole, and P. E. Paré, "A closed-loop framework for inference, prediction, and control of SIR epidemics on networks," *IEEE Transactions on Network Science and Engineering*, vol. 8, no. 3, pp. 2262–2278, 2021.

[11] V. S. Mai, A. Battou, and K. Mills, "Distributed algorithm for suppressing epidemic spread in networks," *IEEE Control Systems Letters*, vol. 2, no. 3, pp. 555–560, 2018.

[12] K. D. Smith and F. Bullo, "Convex optimization of the basic reproduction number," *IEEE Transactions on Automatic Control*, vol. 68, no. 7, pp. 4398–4404, 2023.

[13] V. M. Preciado, M. Zargham, C. Enyioha, A. Jadbabaie, and G. J. Pappas, "Optimal resource allocation for network protection against spreading processes," *IEEE Transactions on Control of Network Systems*, vol. 1, no. 1, pp. 99–108, 2014.

[14] P. Van Mieghem, D. Stevanović, F. Kuipers, C. Li, R. Van De Bovenkamp, D. Liu, and H. Wang, "Decreasing the spectral radius of a graph by link removals," *Physical Review E*, vol. 84, no. 1, p. 016101, 2011.

[15] Q. Ma, Y.-Y. Liu, and A. Olshevsky, "Optimal lockdown for pandemic control," *arXiv preprint arXiv:2010.12923*, 2021.

[16] R. Ofir, F. Bullo, and M. Margaliot, "Minimum effort decentralized control design for contracting network systems," *IEEE Control Systems Letters*, vol. 6, pp. 2731–2736, 2022.

[17] G. Giordano, F. Blanchini, R. Bruno, P. Colaneri, A. D. Filippo, A. D. Matteo, and M. Colaneri, "Modelling the COVID-19 epidemic and implementation of population-wide interventions in Italy," *Nature Medicine*, vol. 26, no. 6, pp. 855–860, 2020.

[18] J. R. Birge, O. Candogan, and Y. Feng, "Controlling epidemic spread: Reducing economic losses with targeted closures," *Management Science*, vol. 68, no. 5, pp. 3175–3195, 2022.

[19] S. M. Kissler, J. R. Fauver, C. Mack, C. Tai, K. Y. Shiue, C. C. Kalinich, S. Jednak, I. M. Ott, C. B. Vogels, J. Wohlgemuth, J. Weisberger, J. DiFiori, D. J. Anderson, J. Mancell, D. D. Ho, N. D. Grubaugh, and Y. H. Grad, "Viral dynamics of sars-cov-2 infection and the predictive value of repeat testing," *medRxiv*, 2020.

[20] C. Viboud, O. N. Bjørnstad, D. L. Smith, L. Simonsen, M. A. Miller, and B. T. Grenfell, "Synchrony, waves, and spatial hierarchies in the spread of influenza," *Science*, vol. 5772, no. 312, p. 447–451, 2006.

[21] D. Brockmann and D. Helbing, "The hidden geometry of complex, network-driven contagion phenomena," *science*, vol. 342, no. 6164, pp. 1337–1342, 2013.

[22] B. A. Butler, R. Stern, and P. E. Paré, "Analysis and applications of population flows in a networked seirs epidemic process," *IEEE Transactions on Network Science and Engineering*, 2024.

[23] L. Sattenspiel and K. Dietz, "A structured epidemic model incorporating geographic mobility among regions," *Mathematical biosciences*, vol. 128, no. 1-2, pp. 71–91, 1995.

[24] D. Balcan, V. Colizza, B. Gonçalves, H. Hu, J. J. Ramasco, and A. Vespignani, "Multiscale mobility networks and the spatial spreading of infectious diseases," *Proceedings of the national academy of sciences*, vol. 106, no. 51, pp. 21 484–21 489, 2009.
[25] M. Kaleta, M. Kęsik-Brodacka, K. Nowak, R. Olszewski, T. Śliwiński, and I. Żółtowska, "Long-term spatial and population-structured planning of non-pharmaceutical interventions to epidemic outbreaks," *Computers & Operations Research*, vol. 146, p. 105919, 2022.
[26] Y. Kang, S. Gao, Y. Liang, M. Li, J. Rao, and J. Kruse, "Multiscale dynamic human mobility flow dataset in the US during the COVID-19 epidemic," *Scientific data*, vol. 7, no. 1, p. 390, 2020.
[27] B. Kalantari, L. Khachiyan, and A. Shokoufandeh, "On the complexity of matrix balancing," *SIAM Journal on Matrix Analysis and Applications*, vol. 18, no. 2, pp. 450–463, 1997.
[28] R. Sinkhorn and P. Knopp, "Concerning nonnegative matrices and doubly stochastic matrices," *Pacific Journal of Mathematics*, vol. 21, no. 2, pp. 343–348, 1967.
[29] A. I. Rikos, T. Charalambous, and C. N. Hadjicostis, "Distributed weight balancing over digraphs," *IEEE Transactions on Control of Network Systems*, vol. 1, no. 2, pp. 190–201, June 2014.
[30] M. Idel, "A review of matrix scaling and sinkhorn's normal form for matrices and positive maps," *arXiv preprint arXiv:1609.06349*, 2016.
[31] M. B. Cohen, A. Madry, D. Tsipras, and A. Vladu, "Matrix scaling and balancing via box constrained newton's method and interior point methods," in 58^{th} *Annual Symposium on Foundations of Computer Science*, 2017, pp. 902–913.
[32] D. G. Luenberger, *Linear and nonlinear programming*. Klewer Academic Publishers, 2021.
[33] X. Chen, H. Qi, L. Qi, and K.-L. Teo, "Smooth convex approximation to the maximum eigenvalue function," *Journal of Global Optimization*, vol. 30, no. 2, pp. 253–270, 2004.
[34] J. R. Magnus, "On differentiating eigenvalues and eigenvectors," *Econometric Theory*, vol. 1, no. 2, p. 179–191, 1985.
[35] J. Nocedal and S. J. Wright, "Quadratic programming," *Numerical optimization*, vol. 35, pp. 448–492, 2006.
[36] M. Zedek, "Continuity and location of zeros of linear combinations of polynomials," *Proceedings of the American Mathematical Society*, vol. 16, no. 1, pp. 78–84, 1965.
[37] Y. Nesterov, *Introductory lectures on convex optimization: A basic course*. Springer Science & Business Media, 2003, vol. 87.
[38] A. Nemirovski and U. Rothblum, "On complexity of matrix scaling," *Linear Algebra and its Applications*, vol. 302, pp. 435–460, 1999.
[39] J. E. Cohen, "Convexity of the dominant eigenvalue of an essentially nonnegative matrix," *Proceedings of the American Mathematical Society*, vol. 81, no. 4, pp. 657–658, 1981.
[40] Y. Tang, G. Qu, and N. Li, "Semi-global exponential stability of augmented primal–dual gradient dynamics for constrained convex optimization," *Systems & Control Letters*, vol. 144, p. 104754, 2020.
[41] Massachusetts Legislature, "2020 Census Data by County," https://malegislature.gov/Redistricting/MassachusettsCensusData/County.
[42] U.S. Bureau of Economic Analysis, "Gross Domestic Product by County, Metro, and Other Areas," https://www.bea.gov/data/gdp/gdp-county-metro-and-other-areas.
[43] e. a. Mitch Smith and, "Us counties covid 19 dataset," 2024. [Online]. Available: https://www.kaggle.com/dsv/8581321
[44] A. Hortaçsu, J. Liu, and T. Schwieg, "Estimating the fraction of unreported infections in epidemics with a known epicenter: An application to covid-19," *Journal of Econometrics*, vol. 220, no. 1, pp. 106–129, 2021.
[45] F. Bullo, *Lectures on Network Systems*, 1.6 ed. Kindle Direct Publishing, 2022. [Online]. Available: https://fbullo.github.io/lns

Mahtab Talaei is currently pursuing her Ph.D. in the Division of Systems Engineering at Boston University in Boston, MA. She obtained her B.Sc. and M.Sc. degrees in Electrical Engineering from Isfahan University of Technology (IUT) in Isfahan, Iran, in 2019 and 2022, respectively. Her research primarily involves utilizing optimization and machine learning techniques to create predictive models for healthcare applications.

Apostolos I. Rikos (M'16) is an Assistant Professor at the Artificial Intelligence Thrust of the Information Hub, The Hong Kong University of Science and Technology (Guangzhou), Guangzhou, China. He is also affiliated with the Department of Computer Science and Engineering, The Hong Kong University of Science and Technology, Clear Water Bay, Hong Kong, China. He received his B.Sc., M.Sc., and Ph.D. degrees in Electrical Engineering from the Department of Electrical and Computer Engineering, University of Cyprus in 2010, 2012, and 2018, respectively. In 2018, he joined the KIOS Research and Innovation Center of Excellence in Cyprus, where he was a Research Lecturer. He joined the Division of Decision and Control Systems at KTH Royal Institute of Technology as a Postdoctoral Researcher in 2020 and the Department of Electrical and Computer Engineering, Division of Systems Engineering, at Boston University as a Postdoctoral Associate in 2023. His research interests are in the areas of distributed optimization and learning, distributed network control and coordination, privacy and security, and algorithmic design.

Alex Olshevsky (Member, IEEE) received the B.S. degrees in Applied Mathematics and Electrical Engineering from the Georgia Institute of Technology, Atlanta, GA, USA, both in 2004, and the M.S. and Ph.D. degrees in electrical engineering and computer science from the Massachusetts Institute of Technology, Cambridge, MA, USA, in 2006 and 2010, respectively. He is currently an Associate Professor with the Department of Electrical and Computer Engineering, Boston University, Boston, MA, USA. His research interests include control systems, optimization, and net- work science. He was the recipient of the National Science Foundation CAREER Award, the Air Force Young Investigator Award, the ICS Prize from INFORMS for best paper on the interface of operations research and computer science, and the SIAM Paper Prize for annual paper from the SIAM Journal on Control and Optimization chosen to be reprinted in SIAM Review.

Laura F. White is a Professor of Biostatistics and Associate Director of the Population Health Data Science Program at the Boston University School of Public Health. She received her BS in Mathematics and Statistics from Utah State University and her PhD in Biostatistics from Harvard University. She co-directs the graduate program in Biostatistics at BU and is an co-director of the Data Science and Surveillance Core of the Center on Emerging Infectious Diseases. Her research interests are in developing novel statistical approaches to understanding infectious disease transmission dynamics and disease burden. Her work is supported by the NIH and CDC.

Ioannis Ch. Paschalidis (Fellow, IEEE) received a diploma in Electrical and Computer Engineering (ECE) from the National Technical University of Athens, Greece, in 1991, and the MS and PhD degrees in Electrical Engineering and Computer Science (EECS), from the Massachusetts Institute of Technology (MIT), Cambridge, Massachusetts, in 1993 and 1996, respectively. In September 1996, he joined Boston University where he has been ever since. He is currently a Distinguished Professor of Engineering and the director of the Hariri Institute for Computing. His current research interests lie in the fields of optimization, control, stochastic systems, robust learning, and computational medicine/biology. His work has been recognized with am NSF CAREER award, several best paper awards, and an IBM/IEEE Smarter Planet Challenge Award. He was an invited participant at the 2002 Frontiers of Engineering Symposium organized by the National Academy of Engineering, at the 2014 National Academies Keck Futures Initiative Conference, and at a 2024 National Academies Symposium on Alzheimer's disease. He is a Fellow of IEEE, IFAC, and the Asia-Pacific AI Association and a distinguished member of the IEEE Control Systems Society. From 2013 to 2019 he was the founding Editor-in-Chief of the IEEE Transactions on Control of Network Systems and he is the General Co-Chair of the 2025 IEEE Conference on Decision and Control.